and HIOS, In: Proceedings of Progress In Electromagnetics Research Symposium, Xi'an, China, March 2010, pp. 531–534.
14. K. Song and Q. Xue, Planar probe coaxial-waveguide power combiner/divider, IEEE Trans Microwave Theory Tech 57 (2009), 2761–2767.
15. L. Chiu and Q. Xue, A parallel-strip ring power divider with high isolation and arbitrary power-dividing ratio, IEEE Trans Microwave Theory Tech 55 (2007), 2419–2426.
16. K. Song and Q. Xue, Compact ultra-wideband (UWB) bandpass filters with multiple notched bands, IEEE Microwave Wireless Compon Lett 20 (2010), 447–449.
17. P.-H. Deng, J.-H. Guo, and W.-C. Kuo, New Wilkinson power dividers based on compact stepped-impedance transmission lines and shunt open stubs, Prog Electromagn Res 123 (2012), 407–426.
18. K. Song and Q. Xue, Novel ultra-wideband (UWB) multilayer slotline power divider with bandpass response, IEEE Microwave Wireless Compon Lett 20 (2010), 13–15.
19. E. Goron, J.-P. Coupez, C. Person, Y. Toutain, H. Lattard, and F. Perrot, Accessing to UMTS filtering specifications using new microstrip miniaturized loop filters, In: Proceedings of 2003 IEEE International Microwave Symposium, Philadelphia, PA, 1599–1602.
20. S.-S. Oh and Y.-S. Kim, A compact duplexer for IMT-2000 handsets using microstrip slow-wave open-loop resonators with high-impedance Meander lines, IEEE Radio Wireless Conference, Waltham, MA, August 2001, pp. 177–180.
21. R.-Y. Yang, Design a high band isolation diplexer for GPS and WLAN system using modified stepped-impedance resonators, Prog Electromagn Res 107 (2010), 101–114.
22. K. Lu, G.-M. Wang, H.-Y. Xu, and X. Yin, Design of a compact planar diplexer based on novel spiral-based resonators, Radio Eng 21 (2012), 528.
23. B. Strassner and K. Chang, Wide-band low-loss high-isolation microstrip periodic-stub diplexer for multiple-frequency applications, IEEE Trans Microwave Theory Tech 49 (2001), 1818–1820.
24. J. Konpang, A compact diplexer using square open loop with stepped impedance resonators, Asia-Pacific Microwave Conference, Macau, 2008, pp. 1–4.
25. S. Srisathit, S. Patisang, R. Phromloungsri, S. Bunnjaweht, S. Kosulvit, and M. Chongcheawchamnan, High isolation and compact size microstrip hairpin diplexer, IEEE Microwave Wireless Compon Lett 15 (2005), 101–103.
26. H.A. Cabral, S.T.G. Bezerra, and M.T. de Melo, A diplexer for UMTS applications, IEEE MTT-S International Microwave and Optoelectronics Conference, Belem, Brazil, 2009, pp. 215–217.
27. K.-H. Li, C.-W. Wang, and C.-F. Yang, A miniaturized diplexer using planar artificial transmission lines for GSM/DCS applications, Asia-Pacific Microwave Conference, Bangkok, Thailand, 2007, pp. 1–4.
28. J. Shi, J.-X. Chen, and Z.-H. Bao, Diplexer based on microstrip line resonators with loaded elements, Prog Electromagn Res 115 (2011), 423–439.
29. C.H. Ahn, Diplexer based on conventional complementary split ring resonator, PhD Thesis, Texas A & M University, College Station, TX, August 2010, pp. 29–35.
30. D. Zayniyev, Miniaturized microstrip Diplexer for Wireless Applications, PhD Thesis, University of Westminster, London, UK, May 2010, pp. 114–127.
31. A. Yatsenko, D. Orlenko, S. Sakhnenko, G. Sevskiy, and P. Heide, A small-size high-rejection LTCC diplexer for WLAN applications based on a new dual-band bandpass filter, IEEE MTT-S International Microwave Symposium Digest, Honolulu, HI, 2007, 2113–2116.
32. P.-H. Deng, C.-H. Wang, and C.-H. Chen, Compact microstrip diplexers based on a dual-passband filter, Asia-Pacific Microwave Conference, Yokohama, Japan, 2006, pp. 1228–1232.
33. F. Cheng, X.-Q. Lin, K. Song, Y. Jiang, and Y. Fan, Compact diplexer with high isolation using the dual-mode substrate integrated waveguide resonator, IEEE Microwave Wireless Compon Lett 23 (2013), 459–461.
34. C.-M. Tsai, S.-Y. Lee, C.-C. Chuang, and C.-C. Tsai, A folded coupled-line structure and its application to filter and diplexer design, IEEE MTT-S International Microwave Symposium Digest, Seattle, WA, June 2002, pp. 1927–1930.
35. X.-W. Chen, W.-M. Zhang, and C.-H. Yao, Design of microstrip diplexer with wide band-stop, International Conference on Microwave and Millimeter Wave Technology, 2007, Builin, pp. 1–3.
36. A.-F. Sheta, J.-P. Coupez, G. Tanne, S. Toutain, and J.-P. Blot, Miniature microstrip stepped impedance resonator bandpass filters and diplexers for mobile communications, IEEE MTT-S International Microwave Symposium Digest, San Francisco, CA, June 1996, pp. 607–610.
37. L. Yo-Shen, C. Po-Ying, and L. Chun-Lin, Compact parallel-coupled microstrip diplexers with good stopband rejection, Asia-Pacific Microwave Conference, Singapore, December 2009, pp. 2621–2624.
38. G. Tudosie and R. Vahldieck, An efficient design approach for planar microwave multiplexers, 34th European Microwave Conference, Amsterdam, The Netherlands, October 2004, pp. 1229–1232.
39. C.-S. Ye, Y.-K. Su, M.-H. Weng, and C.-Y. Hung, A microstrip ring-like diplexer for Bluetooth and ultra wide band (UWB) application, Microwave Opt Technol Lett 51 (2009), 1518–1520.
40. C.-Y. Huang, M.-H. Weng, C.-S. Ye, and Y.-X. Xu, A high band isolation and wide stopband diplexer using dual-mode stepped-impedance resonators, Prog Electromagn Res 100 (2010), 299–308.
41. J.-S. Hong and M.J. Lancaster, Microstrip filters for RF/microwave applications, Chapter 8, Wiley, 2001, pp. 235–271.
42. M.-M. Abu Hussain, An E-band diplexer for gigabit wireless communications systems, Islamic University, Gaza, 2013, p. 25.
43. Ansoft High Frequency Structure Simulator version 13.0. Ansoft Corp., Pittsburgh, PA.
44. Zeland Software, Inc., IE3D version 12, Zeland Software, Fremont, CA.

IMPACT ANALYSIS ON DISTANCE VARIATION BETWEEN PATCH ANTENNA AND METAMATERIAL

Pankaj Katiyar and Wan Nor Liza Wan Mahadi
EMRD, Department of Electrical Engineering, Faculty of Engineering, University of Malaya (UM), 50603 Kuala Lumpur, Malaysia;
Corresponding author: pankaj.katiyar@siswa.um.edu.my

Received 30 May 2014

ABSTRACT: *Metamaterials are artificially engineered material having negative permittivity and permeability. Due to their negative constitutive parameters, metamaterials are capable of focusing incident electromagnetic energy called as beam focusing property. We have made use of beam focusing property of metamaterial to enhance antenna far-field gain. We have also conducted experimental study by varying the distance between patch antenna and metamaterial array to determine optimum distance. The distance is varied in seven steps of 35 mm. The far-field gain of antenna is increased by 4 dB when metamaterial is placed at 95 mm. The beamwidth of antenna reduces when loaded with metamaterial indicating beam sharpening. At 155 mm from patch antenna, the beamwidth reduces to 33.95° and starts increasing as metamaterial is moved further away. The resonance frequency and bandwidth of antenna follows alternate increase and decrease pattern as the distance of metamaterial is increased, however, the impact is negligible.* © 2015 Wiley Periodicals, Inc. Microwave Opt Technol Lett 57:178–183, 2015; View this article online at wileyonlinelibrary.com. DOI 10.1002/mop.28809

Key words: *metamaterial; split ring resonator; gain enhancement; CLS; microstrip patch*

1. INTRODUCTION

Recently, extensive research is performed on enhancing performance of antenna using metamaterial structure. These antenna are

Conflict of interest: I declare no conflict of interest. This work was not supported by any sponsors.

modified in many different ways for performance enhancement using metamaterial [1–5]. Metamaterial is artificially engineered structure or material which exhibits negative permittivity and negative permeability. Metamaterials gain their property from its structure. All the metamaterial cells used for antenna enhancement are fabricated on PCB substrate.

In 1968, Veselago theoretically explained materials capable of having negative permeability and permittivity [6]. Due to negative constitutive parameter, the wave flowing through the metamaterial is antiparallel to the phase velocity. It was Pendry [7] who demonstrated the first prototype of metamaterial with negative permittivity and permeability using array of thin conducting wires. This array of thin wire when excited with electromagnetic energy at plasma frequency generates plasmon which results in negative permittivity and permeability. The generation of plasmon also relates to unique properties such as reversal of Doppler effect, reversal of snells law, and so forth [8].

Ran et al. [9] did series of experimental verification on several metamaterial structure. In their experiment, they demonstrated beam focusing, power transmission, prism refraction, and beam shifting property of metamaterial. Due to such unique property, metamaterial finds many different application including antenna performance enhancement, SAR reduction, space communication, commercial equipment, and medical [10]. One of the such unique application of metamaterial is noninvasive measurement of vital signals from human body [11]. In their research, they made use of highly directional metamaterial antenna and directed electromagnetic energy toward the human body and made respiration measurement by measuring received signal from human body.

In this research, the CLS loaded split ring resonator (SRR) metamaterial is used to enhance performance of rectangular patch antenna. The beam focusing property demonstrated by Ran et al., is used by placing metamaterial array in front of antenna. The distance between patch antenna and metamaterial array is varied in seven steps of 35 mm each. At each step, a full three-dimensional (3D) measurement is performed. The measured result of antenna and antenna with metamaterial at each step is compared against far-field gain, 3-dB beamwidth, bandwidth, and resonance frequency. An impact analysis on each of the parameter is explained.

2. RESEARCH METHODOLOGY

This section provides details of research methodology and tools used in conducting this research. The flow diagram of research is as shown in Figure 1.

The regular rectangular patch antenna is first simulated in computer simulation technology (CST). The rectangular patch antenna is matched using quarter wavelength impedance matching technique and fed with microstrip line. CST is also used to simulated single cell of CLS loaded SRR metamaterial. Single cell is tuned to have negative properties at 2.45 GHz and above. This single cell structure is then used to form 13 × 5 array of metamaterial.

The metamaterial array is placed in front of antenna and further study to analyze its impact is conducted. The distance between patch antenna and metamaterial array is varied from 35 to 215 mm marked as H7 to H1, respectively. At each point, detailed study on far-field gain, beamwidth, resonance frequency, and bandwidth is performed.

The model is then fabricated for experimental verification purpose. Two samples are created to determine sample to sample to variation. The fabricated model is tested for 3D data in fully anechoic chamber.

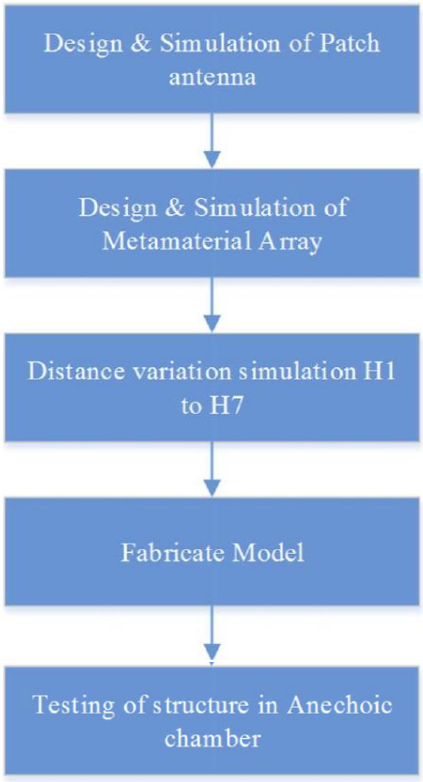

Figure 1 Research methodology. [Color figure can be viewed in the online issue, which is available at wileyonlinelibrary.com]

3. MICROSTRIP PATCH ANTENNA

Microstrip patch first came into existence in 1980, and received attention due to their compactness [12]. As patch antenna are extensively studied, it is easy to design one with the help of standardized formulas. Simulation tools like CST provide easy step by step guide to design microstrip-fed rectangular patch antenna.

Above Figure 2 shows the simulated rectangular patch antenna resonating at 2.442 GHz. Total size of patch antenna is 55.42 × 75.22 mm^2, with rectangular patch of 46 × 38.20 mm^2. The impedance of rectangular patch is matched using quarter wavelength microstrip line of 0.60 mm in width and 21.50 mm in length. Additionally, antenna is equipped with PI matching network for further tuning if required. Patch antenna is fabricated on Rogers RO5870T substrate with dielectric constant of 2.3. The simulated *S*-parameter of antenna is as shown in Figure 3.

4. METAMATERIAL

The elementary cell of the proposed multilayer metamaterial is shown in Figure 4 [13]. It is similar to regular SRR but in addition has two I shape strips adjacent to split ring. The I shape capacitive strip is 15.10 mm in length and 13.1 mm wide. The gap between two capacitive strips is 0.5 mm. The outer ring of

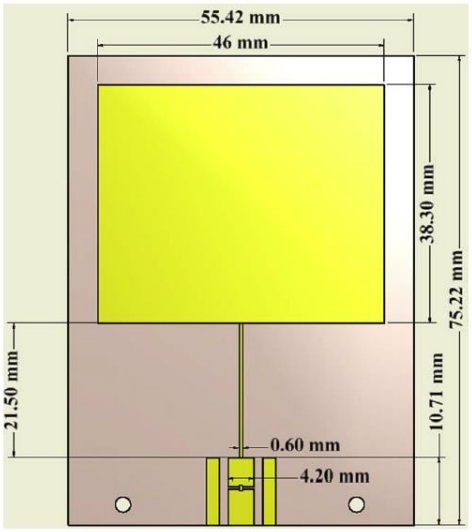

Figure 2 Rectangular microstrip patch antenna. [Color figure can be viewed in the online issue, which is available at wileyonlinelibrary.com]

SRR is 9.10 mm while inner ring is 7.10 mm. CLS-loaded SRR has the advantage of SRR and I pattern single-cell metamaterial. Additional I pattern increased the amount of capacitance exponentially. The coupling of I pattern to I pattern and I pattern to outer ring brings the resonance frequency down.

The single cell of CLS-loaded SRR is then used to form multilayer array of metamaterial as shown in Figure 5. The array consists of 13 strips of metamaterial, where each strip consists of five CLS-loaded SRR structure. The total size of multilayer array is $161.50 \times 31 \times 92.50\ \text{mm}^3$.

5. DISTANCE VARIATION

Ran [9] in his research demonstrated beam focusing property of metamaterial which is similar to optical lens focusing incident light on lens. Similarly, the multilayer array of metamaterial when excited with electromagnetic energy will focus the electromagnetic beam resulting in enhancement of antenna performance.

The multilayer metamaterial shown in above Figure 5 is placed in front of rectangular patch antenna as shown in Figure 6.

The platform is made up of 4-mm thick acrylic to hold antenna and metamaterial in place. The proposed platform has

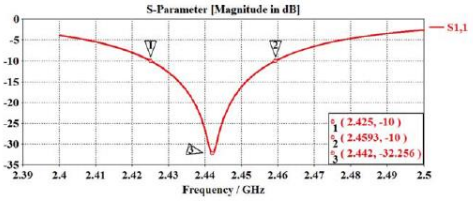

Figure 3 Simulated *S*-parameter of patch antenna. [Color figure can be viewed in the online issue, which is available at wileyonlinelibrary.com]

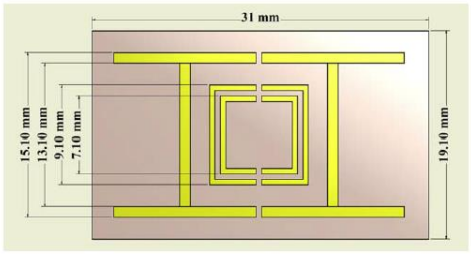

Figure 4 CLS-loaded SRR metamaterial cell. [Color figure can be viewed in the online issue, which is available at wileyonlinelibrary.com]

holes and slots to keep metamaterial array in place during 3D measurement. The holes are marked H1 to H7 at which 3D measurement is performed for gain and beamwidth of antenna. The patch antenna is placed vertically with the help of two 90° bend. Additional support bar on top is provided to compensate for bending due to weight of metamaterial array. The distance between each marked holes is 35 mm.

The 3D model is created using Autodesk Inventor and then simulated in CST. The final simulated model is fabricated. Simulation is performed at each marked location from H1 to H7. At each point, antenna far-field gain, beamwidth, bandwidth, and resonance frequency is recorded. Final conclusion is drawn on verification from measurement.

6. RESULTS AND DISCUSSION

The model shown in Figure 6 is fabricated for further investigation. The fabrication model is measured against simulation results in fully anechoic chamber. 3D measurement and *S*-parameter measurement is performed for all the points from H1 to H7.

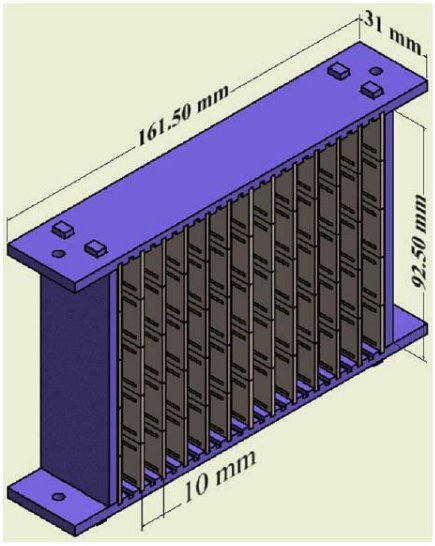

Figure 5 Metamaterial array. [Color figure can be viewed in the online issue, which is available at wileyonlinelibrary.com]

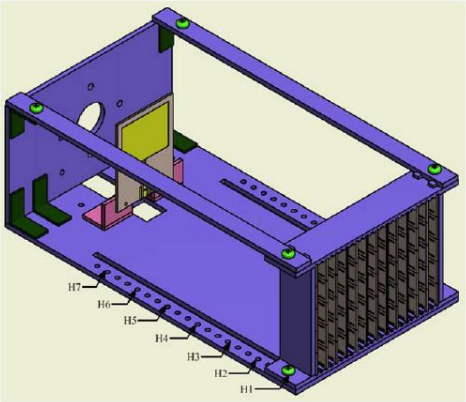

Figure 6 Three-dimensional model of antenna with metamaterial array. [Color figure can be viewed in the online issue, which is available at wileyonlinelibrary.com]

The simulated rectangular patch antenna with quarter wavelength matching has resonance frequency of 2.442 GHz. The fabricated model on Rogers RO5870T is resonating at 2.462 and 2.461 GHz. The measured resonance frequency is consistent for the both the fabricated sample as shown in Figure 7, however, the difference in simulated resonance frequency to measured is due to fabrication tolerance.

The 3D measurement is performed for antenna only which serves as baseline for comparing antenna gain with metamaterial. Figure 8 shows the simulated and measured far-field polar plot of patch antenna as measured in anechoic chamber. The measured far-field gain of antenna is 5.8 and 5.71 dBi as compared to simulated gain of 6.3 dBi.

For the next set of testing, metamaterial array is fixed at H1 and measurements are performed. H1 is located at 215 mm from patch antenna. Similarly, metamaterial array is placed at H2 and then measurement is performed again. This measurement continues until point H7 and all the results are tabulated for easy comparison. The measured result is divided into four blocks as far field, beamwidth, bandwidth, and resonance frequency. An average value of Sample 1 and Sample 2 is used here after for comparison.

6.1. Far-Field Gain

Figure 9 shows the simulated versus measured far-field gain of antenna. The patch antenna has measured gain of 5.76 dBi as against simulated of 6.3 dBi. The gain of patch antenna

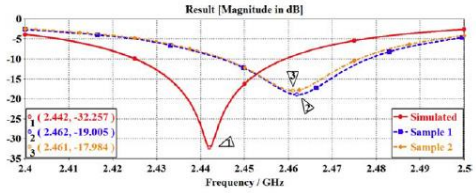

Figure 7 Measurement versus simulated *S*-parameter of patch antenna. [Color figure can be viewed in the online issue, which is available at wileyonlinelibrary.com]

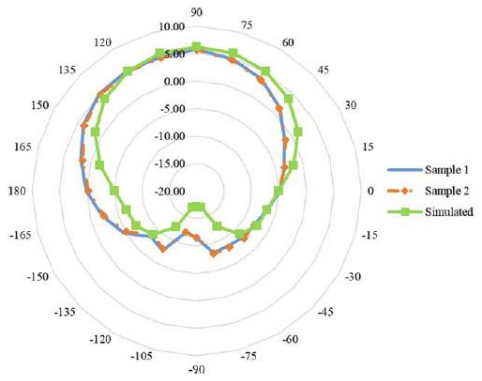

Figure 8 Three-dimensional measurement versus simulated of patch antenna. [Color figure can be viewed in the online issue, which is available at wileyonlinelibrary.com]

increases to 6.91 dBi when metamaterial array is placed at H7 point.

The far-field gain of antenna continues to increase until point H5, where it reaches maximum of 9.84 dBi giving a total increase in gain of 4.08 dB. As metamaterial is moved further away from antenna gain starts reducing but still at higher value as compared to patch antenna. At point H1 which is 215 mm from patch antenna, the gain of antenna is 8.82 dBi.

6.2. Beamwidth

Antenna beamwidth is measured in degrees in-between the two half power points (3 dB) of the major lobe of the antenna. Three decibel beamwidth of antenna provides information on directional property of antenna. The measured 3D beamwidth of rectangular patch antenna is 87.48° which is close to simulated value.

When metamaterial is introduced the 3-dB beamwidth starts reducing. At H7, the measured 3-dB beamwidth of antenna is 73.41°. The beamwidth of antenna continues to reduce until point H1 reaching 34.71°. The reduction in beamwidth indicates that the radiation beam is becoming sharper as distance of metamaterial array from patch antenna is increased. At point H3 which is 155 mm from patch antenna, the 3-dB beamwidth is 33.94° which is smallest, indicating sharpest radiation beam.

6.3. Bandwidth

IEEE defines bandwidth as "The range of frequencies within which the performance of the antenna is acceptable." Here, in our research, −10 dB bandwidth is considered acceptable and

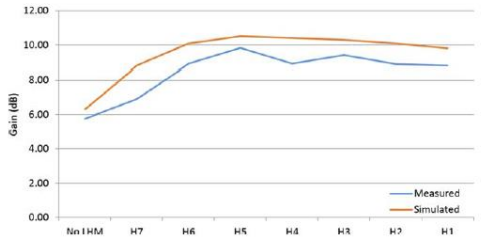

Figure 9 Measurement versus simulated far-field gain. [Color figure can be viewed in the online issue, which is available at wileyonlinelibrary.com]

Link to Full-Text Articles :

http://onlinelibrary.wiley.com/doi/10.1002/mop.28809/full